Electronic Supplementary Material (ESI) for Dalton Transactions.

Supporting information

IR- spectra.

Table S1 IR-spectra (cm^{-1} in KBr) of starting compounds and complexes **1-4**.

	{CpMo $(CO)_3\}_2$	{Cp*Mo $(CO)_2\}_2$	PPN·Cl	C_{60}	C_{70}	(PPN$^+$) {CpMo$(CO)_2$ (η^2-C_{60})}$^-$ (**1**)	(PPN$^+$) {CpMo$(CO)_2$ (η^2-C_{70})}$^-$·C_6H_{14} (**2**)	(PPN$^+$) {Cp*Mo$(CO)_2$ (η^2-C_{60})}$^-$ ·C_6H_5CN ·$C_6H_4Cl_2$ (**3**)	(PPN$^+$) {CpMo$(CO)_3\}^-$ (**4**)
Cp(*) Mo$(CO)_x$, x = 2, 3	417w 451m 477w 501m 547m 587m 824s 1016w 1264w 1419w 1427w C=O 1886s 1899s 1953s C-H 3095w 3115w	448w 482w 495m 531s 1027m 1384s 1416w 1450w 1478w C=O 1825s 1870s C-H 2861w 2908w 2970w				- 437w - 495m* 546m* - - 1026w* 1282s* - - C=O 1798s 1819s 1888s C-H 3088w -	- 438w 454w* 497m* 540m 580w* - - 1283s* 1414m* 1433m C=O - 1812s 1898s C-H 3091w -	- 438w 484w 503s* 532s* 1025w* - - 1281s* 1454m* 1481w* C=O 1787s 1878s C-H 2853w 2924w 2961w	- 447w 461w 502s* 542m* 616m - - 1272s* - - C=O 1768s 1786s 1895s C-H 3088w
PPN$^+$			500s 531s 550s 694m 724m 746m 754m 997m 1024w 1075w 1115s 1262s - - 1439s 1483m 1587m 3046w			495m* 531s* 546m* 690s 722s 752w - 998m 1026w 1074w 1113s 1282s* 1300m 1319m 1436s 1479w 1587w 3057w	497m* 533s 545m 691s 721s* 743w* - 998w 1026w 1089w* 1114s 1283s* 1298m 1318m 1438m 1482w 1588w 3056w	503s* 532s* 546m 689s 722s 744w 753w 998m 1025w* 1070w 1114s 1261s 1281s* 1300m 1436s 1481w* 1587w 3054w	502s* 535s 542m* 693s 723s 752m 758m 998m 1027w 1072w 1117s 1272s* 1289s 1303s 1438s 1482m 1586w 3055w
Fullerene				C_{60} 526s - 576m - 1182m 1429s	C_{70} 457w 534s 564m 576s - 642m 673m 794m 1132w - 1413w 1429s	Coord. C_{60} 531s* 566w 576w 582w 1182m 1402w 1416s	Coord. C_{70} 454w* 530s 567w 580w* 607w 639w 672w 791m - 1406m 1414m* 1426s*	Coord. C_{60}^- 532m* 576m 1183m 1392s 1412w	
Solvent							C_6H_{14} 721s* 743w* 1089w* - 1462w 2926w 2951w	$C_6H_4Cl_2$ - 740w 1025w* 1454m*	

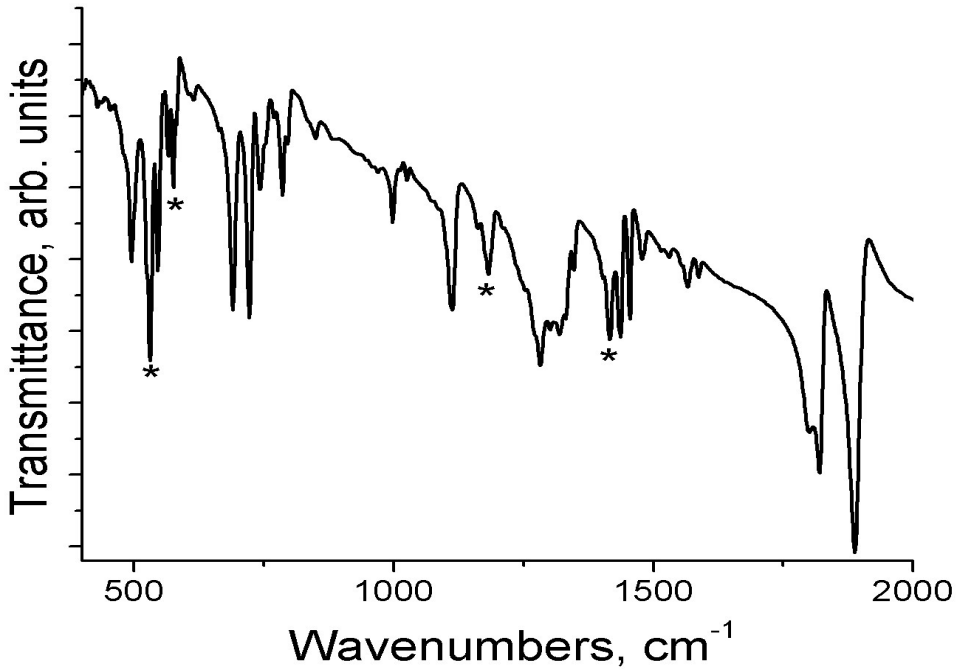

Fig. S1 IR-spectrum of $(PPN^{+})\{CpMo(CO)_2(\eta^2\text{-}C_{60})\}^{-}$ (**1**) in KBr pellet prepared in anaerobic conditions. Absorption bands of C_{60} are marked by asterisks.

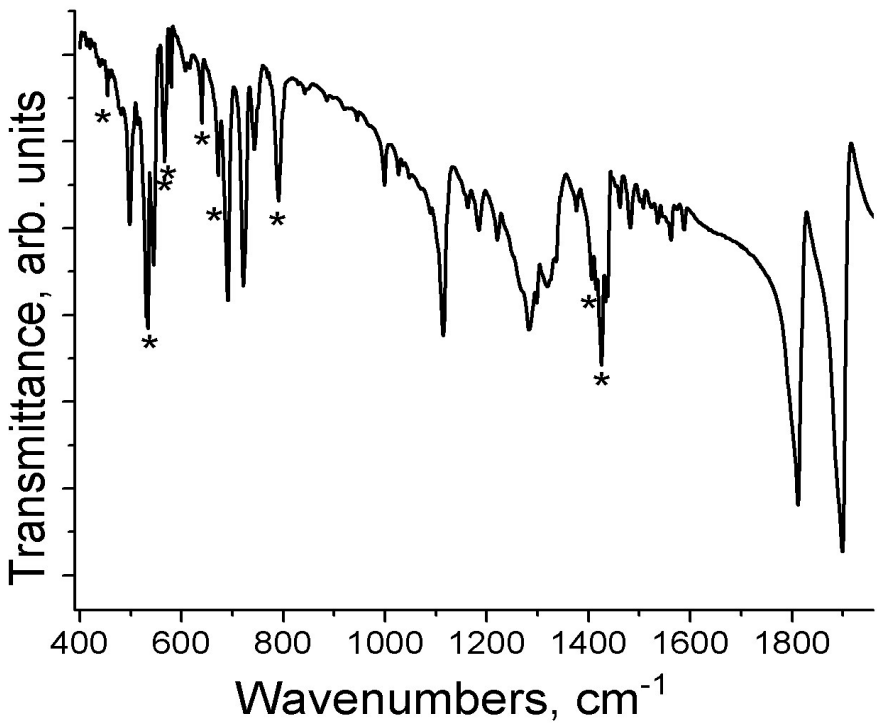

Fig. S2 IR-spectrum of $(PPN^{+})\{CpMo(CO)_2(\eta^2\text{-}C_{70})\}^{-}\cdot C_6H_{14}$ (**2**) in KBr pellet prepared in anaerobic conditions. Absorption bands of C_{70} are marked by asterisks.

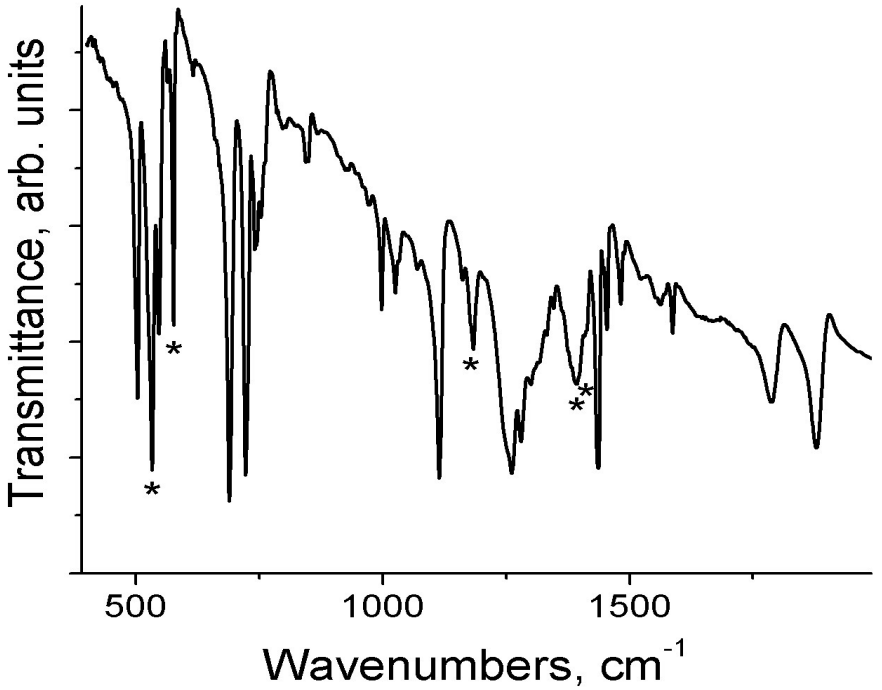

Fig. S3 IR-spectrum of $(PPN^{+})\{Cp^{*}Mo(CO)_2(\eta^2\text{-}C_{60})\}^{-}\cdot C_6H_4Cl_2\cdot C_6H_5CN$ (**3**) in KBr pellet prepared in anaerobic conditions. Absorption bands of C_{60} are marked by asterisks.

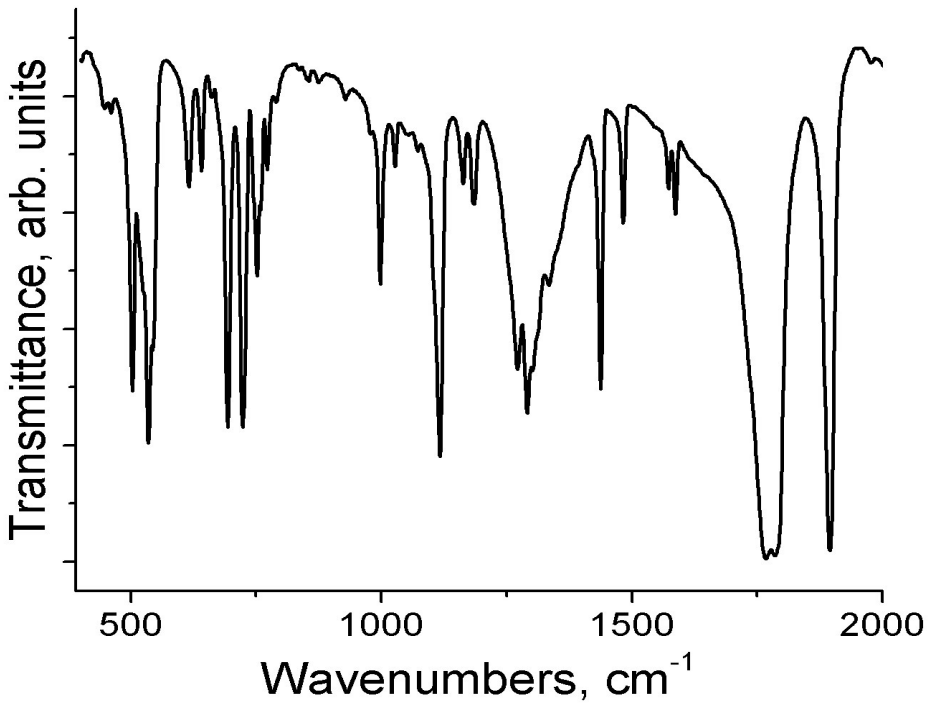

Fig. S4 IR-spectrum of $(PPN^{+})\{CpMo(CO)_3\}^{-}$ (**4**) in KBr pellet prepared in anaerobic conditions.

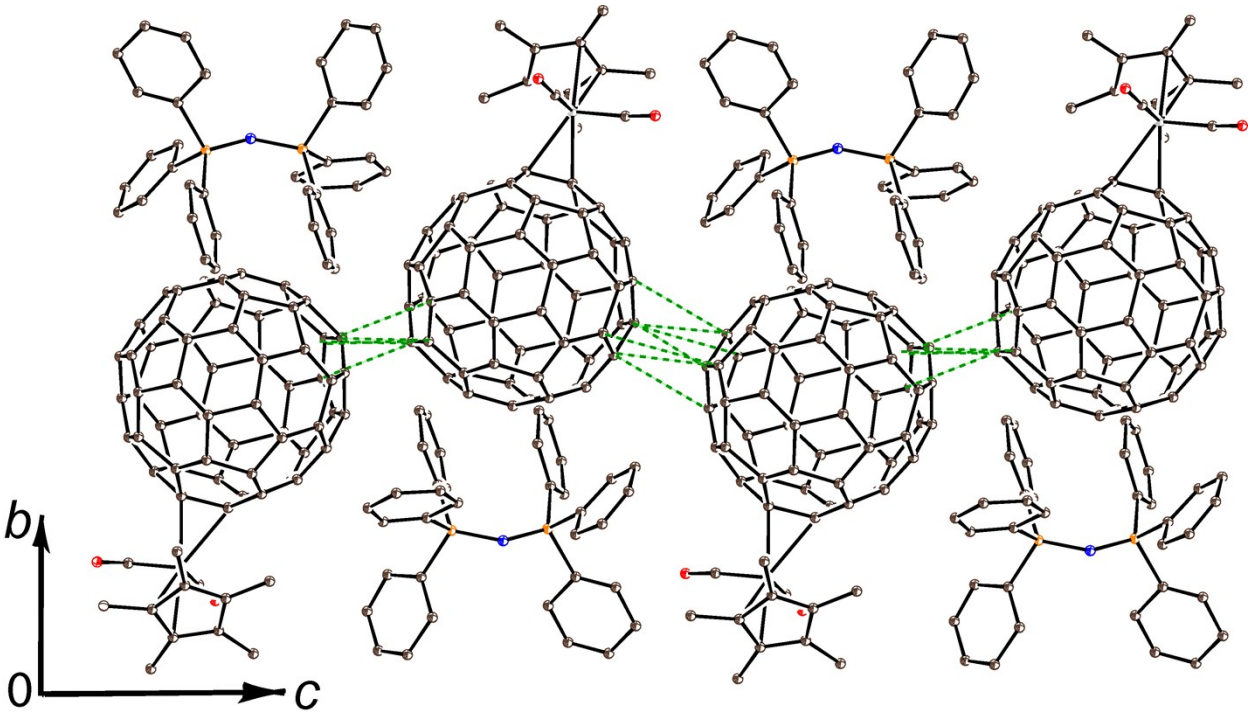

Fig. S5 View on zigzag fullerene chains in complex **3** arranged along the *c* axis and formed by closely packed $\{Cp^*Mo(CO)_2(\eta^2\text{-}C_{60})\}^-$ anions.

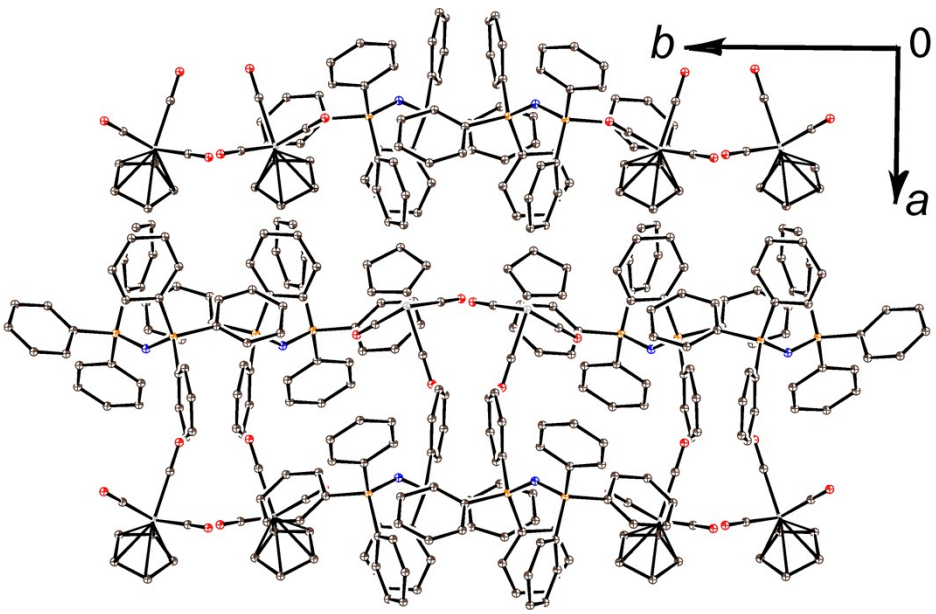

Fig. S6 View on the crystal structure of $(PPN^+)\{CpMo(CO)_3\}^-$ (**4**) along the *c* axis.

Data of EPR spectra for complex 3.

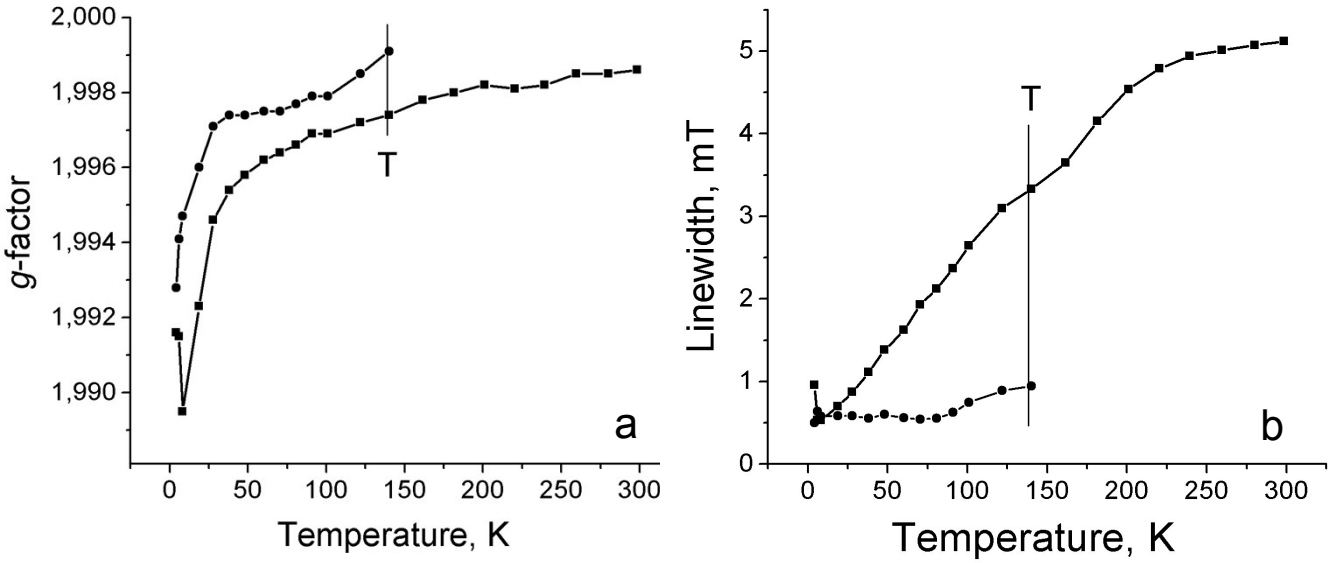

Fig. S7 Temperature dependence of *g*-factor (a) and linewidth (b) of EPR signal from polycrystalline complex **3**. T marks the temperature of splitting of EPR signal.

Theoretical calculations

Table S2. Calculated state, total energies (E), relative energies (ΔE), $<S^2>$ values, and number of imaginary frequencies (NImag.) of the singlet and triplet states in $\{CpMo(CO)_2(\eta^2\text{-}C_{60})\}^-$ and $\{Cp^*Mo(CO)_2(\eta^2\text{-}C_{60})\}^-$ at the CAM-B3LYP-D3 and M11/cc-pVTZ-PP/cc-pVDZ levels of theory

Method[a]	State	E / hartree	ΔE / eV	$<S^2>$	NImag.
$\{CpMo(CO)_2(\eta^2\text{-}C_{60})\}^-$					
RCAM-B3LYP-D3	^1A	−2773.3329	–	0	0
RM11	^1A	−2773.1358	–	0	0
RCAM-B3LYP-D3	^1A	−2773.2421	0	0	–[b]
UCAM-B3LYP-D3	^3A	−2773.1923	1.35	2.025	–[b]
RM11	^1A	−2773.0376	0.00	0	–[b]
UM11	^3A	−2772.9910	1.27	2.031	–[b]
$\{Cp^*Mo(CO)_2(\eta^2\text{-}C_{60})\}^-$					
RCAM-B3LYP-D3	^1A	−2969.8076	0	0	0
UCAM-B3LYP-D3	^3A	−2969.7809	0.73	2.024	0
RM11	^1A	−2969.5867	0	0	0
UM11	^3A	−2969.5633	0.63	2.030	0
RCAM-B3LYP-D3	^1A	−2969.1740	0	0	–[b]
UCAM-B3LYP-D3	^3A	−2969.1367	1.02	2.045	–[b]
RM11	^1A	−2968.9446	0	0	–[b]
UM11	^3A	−2968.9095	0.95	2.040	–[b]

[a] The cc-pVTZ-PP and cc-pVDZ basis sets were used for molybdenum and the other atoms, respectively.
[b] X-ray structure was used without geometry optimization.

Table S3. Observed and calculated bond lengths and Wiberg bond indices of the ^1A state in $\{CpMo(CO)_2(\eta^2\text{-}C_{60})\}^-$ at the RCAM-B3LYP-D3 and RM11/cc-pVTZ-PP/cc-pVDZ levels of theory

	Bond length, Å			Wiberg bond index	
	Obs.	RCAM-B3LYP-D3	RM11	RCAM-B3LYP-D3	RM11
Mo1−C61	2.368(2)	2.414	2.434	0.281	0.273
Mo1−C62	2.354(3)	2.356	2.371	0.334	0.326
Mo1−C63	2.351(3)	2.330	2.345	0.355	0.342
Mo1−C64	2.369(3)	2.356	2.371	0.334	0.326
Mo1−C65	2.392(3)	2.414	2.434	0.281	0.273
Mo1−C66	1.943(3)	1.946	1.942	1.325	1.310
Mo1−C67	1.947(3)	1.946	1.942	1.325	1.310
C66−O1	1.157(3)	1.163	1.159	2.013	2.033
C67−O2	1.164(3)	1.163	1.159	2.013	2.033
Mo1−C9	2.252(2)	2.234	2.220	0.572	0.586
Mo1−C1	2.241(2)	2.234	2.220	0.572	0.586
C9−C1	1.497(3)	1.509	1.516	0.976	0.961
C9−C10	1.478(3)	1.484	1.486	1.062	1.058
C9−C8	1.480(3)	1.482	1.484	1.057	1.052
C1−C2	1.475(3)	1.484	1.486	1.062	1.058
C1−C5	1.483(3)	1.482	1.484	1.057	1.052
Total of Mo				6.035	5.963

Table S4. Observed and calculated bond lengths and Wiberg bond indices of the ^1A state in $\{Cp^*Mo(CO)_2(\eta^2\text{-}C_{60})\}^-$ at the RCAM-B3LYP-D3 and RM11/cc-pVTZ-PP/cc-pVDZ levels of theory

	Bond length, Å			Wiberg bond index	
	Obs.	RCAM-B3LYP-D3	RM11	RCAM-B3LYP-D3	RM11
Mo1B−C1B	2.306(7)	2.344	2.359	0.329	0.315
Mo1B−C2B	2.450(6)	2.447	2.464	0.258	0.248
Mo1B−C3B	2.513(7)	2.447	2.462	0.258	0.252
Mo1B−C4B	2.415(7)	2.344	2.351	0.329	0.324
Mo1B−C5B	2.284(7)	2.305	2.317	0.346	0.332
Mo1B−C11B	1.815(16)	1.940	1.931	1.329	1.332
Mo1B−C12B	1.943(14)	1.940	1.942	1.329	1.296
C11B−O1B	1.23(2)	1.164	1.162	1.998	2.011
C12B−O2B	1.228(16)	1.164	1.160	1.998	2.028
Mo1B−C302	2.385(13)	2.247	2.236	0.549	0.560
Mo1B−C307	2.205(11)	2.247	2.229	0.549	0.568
C302−C307	1.525(19)	1.511	1.518	0.974	0.959
C302−C301	1.476(17)	1.481	1.482	1.068	1.064
C302−C303	1.421(17)	1.482	1.484	1.059	1.054
C307−C314	1.466(17)	1.481	1.484	1.068	1.062
C307−C315	1.528(17)	1.482	1.483	1.059	1.055
Total of Mo				6.016	5.942

Table S5. Observed and calculated bond lengths and Wiberg bond indices of the ^3A state in $\{Cp^*Mo(CO)_2(\eta^2\text{-}C_{60})\}^-$ at the UCAM-B3LYP-D3 and UM11/cc-pVTZ-PP/cc-pVDZ levels of theory

	Bond length, Å			Wiberg bond index	
	Obs.	UCAM-B3LYP-D3	UM11	UCAM-B3LYP-D3	UM11
Mo1B−C1B	2.306(7)	2.355	2.359	0.314	0.307
Mo1B−C2B	2.450(6)	2.408	2.410	0.269	0.265
Mo1B−C3B	2.513(7)	2.397	2.397	0.275	0.273
Mo1B−C4B	2.415(7)	2.338	2.340	0.340	0.334
Mo1B−C5B	2.284(7)	2.317	2.323	0.349	0.340
Mo1B−C11B	1.815(16)	1.985	1.998	1.172	1.125
Mo1B−C12B	1.943(14)	1.970	1.973	1.189	1.160
C11B−O1B	1.23(2)	1.153	1.148	2.087	2.128
C12B−O2B	1.228(16)	1.154	1.151	2.078	2.105
Mo1B−C302	2.385(13)	2.306	2.267	0.455	0.485
Mo1B−C307	2.205(11)	2.234	2.209	0.525	0.553
C302−C307	1.525(19)	1.465	1.472	1.103	1.083
C302−C301	1.476(17)	1.486	1.489	1.044	1.032
C302−C303	1.421(17)	1.485	1.489	1.043	1.032
C307−C314	1.466(17)	1.487	1.490	1.039	1.031
C307−C315	1.528(17)	1.489	1.492	1.035	1.028
Total of Mo				5.453	5.381

Table S6. Sum of charge densities for the ^1A and ^3A states in $\{CpMo(CO)_2(\eta^2\text{-}C_{60})\}^-$ and $\{Cp^*Mo(CO)_2(\eta^2\text{-}C_{60})\}^-$ by Mulliken and natural population analyses at the CAM-B3LYP-D3 and M11/cc-pVTZ-PP/cc-pVDZ levels of theory[a].

	^1A state		^3A state	
	Mulliken	NPA[b]	Mulliken	NPA[b]
$\{CpMo(CO)_2(\eta^2\text{-}C_{60})\}^-$				
CAM-B3LYP-D3				
Mo1	−0.589	−0.892		
C66−O1	0.121	0.250		
C67−O2	0.121	0.250		
Cp	0.084	0.029		
C_{60}	−0.737	−0.638		
M11				
Mo1	−0.469	−0.916		
C66−O1	0.112	0.284		
C67−O2	0.112	0.284		
Cp	0.044	−0.005		
C_{60}	−0.799	−0.648		
$\{Cp^*Mo(CO)_2(\eta^2\text{-}C_{60})\}^-$				
CAM-B3LYP-D3				
Mo1B	−0.453	−0.815	−0.411	−0.533
C11B−O1B	0.113	0.241	0.180	0.300
C12B−O2B	0.113	0.241	0.182	0.289
Cp*	0.048	0.018	0.216	0.107
C_{60}	−0.822	−0.686	−1.166	−1.163
M11				
Mo1B	−0.373	−0.842	−0.360	−0.542
C11B−O1B	0.096	0.268	0.178	0.346
C12B−O2B	0.106	0.286	0.186	0.326
Cp*	0.042	−0.020	0.223	0.076
C_{60}	−0.869	−0.692	−1.227	−1.206

[a] Geometry optimization was carried out.
[b] Natural population analysis.

Table S7. Observed and calculated frequencies (cm^{-1}) of CO stretching mode of the ^1A states in $\{CpMo(CO)_2(\eta^2\text{-}C_{60})\}^-$ and $\{Cp^*Mo(CO)_2(\eta^2\text{-}C_{60})\}^-$ at the RCAM-B3LYP-D3 and RM11/cc-pVTZ-PP/cc-pVDZ levels of theory.

Obs.	Calc.[a]	
	RCAM-B3LYP-D3	RM11
$\{CpMo(CO)_2(\eta^2\text{-}C_{60})\}^-$		
1798	1820	1822
1819	1879	1877
1888		
$\{Cp^*Mo(CO)_2(\eta^2\text{-}C_{60})\}^-$		
1787	1807	1808
1878	1868	1866

[a] The calculated frequencies at RCAM-B3LYP-D3 and RM11/cc-pVTZ-PP/cc-pVDZ levels are scaled by 0.9303 and 0.9244, respectively.

Table S8. Sum of spin densities for the ^3A state[a] in $\{Cp^*Mo(CO)_2(\eta^2\text{-}C_{60})\}^-$ by Mulliken and natural population analyses at the UCAM-B3LYP-D3 and UM11/cc-pVTZ-PP/cc-pVDZ levels of theory.

	UCAM-B3LYP-D3		UM11	
	Mulliken	NPA[b]	Mulliken	NPA[b]
Mo1B	0.813	0.783	0.830	0.805
C11B−O1B	0.118	0.109	0.099	0.093
C12B−O2B	−0.010	−0.004	−0.011	−0.006
Cp*	0.068	0.082	0.067	0.079
C_{60}	1.011	1.030	1.015	1.029

[a] Geometry optimization was carried out. [b] Natural population analysis.

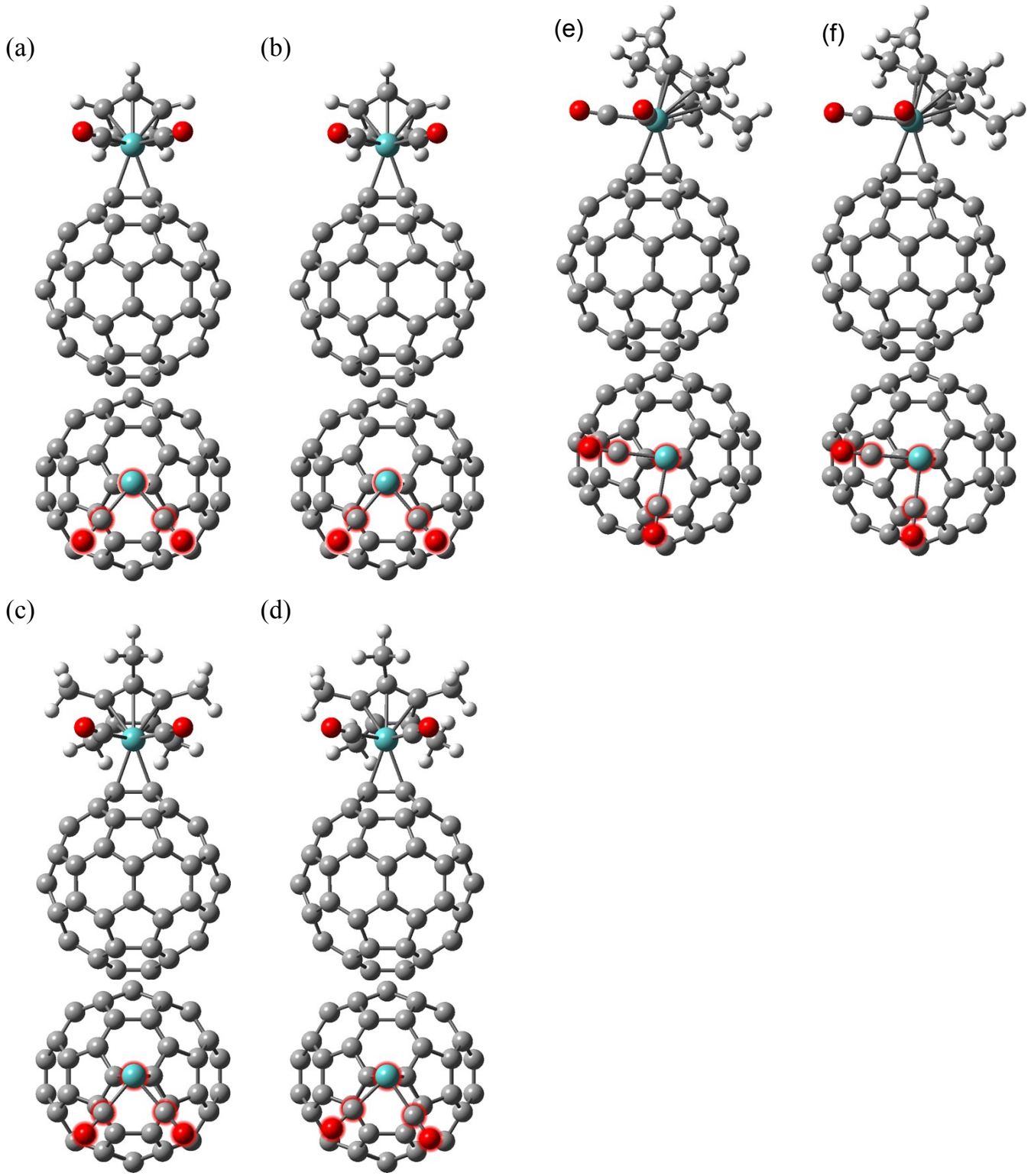

Fig. S8 Optimized structures: $\{CpMo(CO)_2(\eta^2\text{-}C_{60})\}^-$ in the ^1A states at the (a) RCAM-B3LYP-D3 and (b) RM11; $\{Cp^*Mo(CO)_2(\eta^2\text{-}C_{60})\}^-$ in the ^1A states at the (c) RCAM-B3LYP-D3 and (d) RM11, and the ^3A states at the (e) UCAM-B3LYP-D3 and (f) UM11/cc-pVTZ-PP/cc-pVDZ levels of theory. In the top view, cyclopentadienyl and pentamethylcyclopentadienyl ligands are omitted, and $Mo(CO)_2$ moiety is highlighted for clarity.

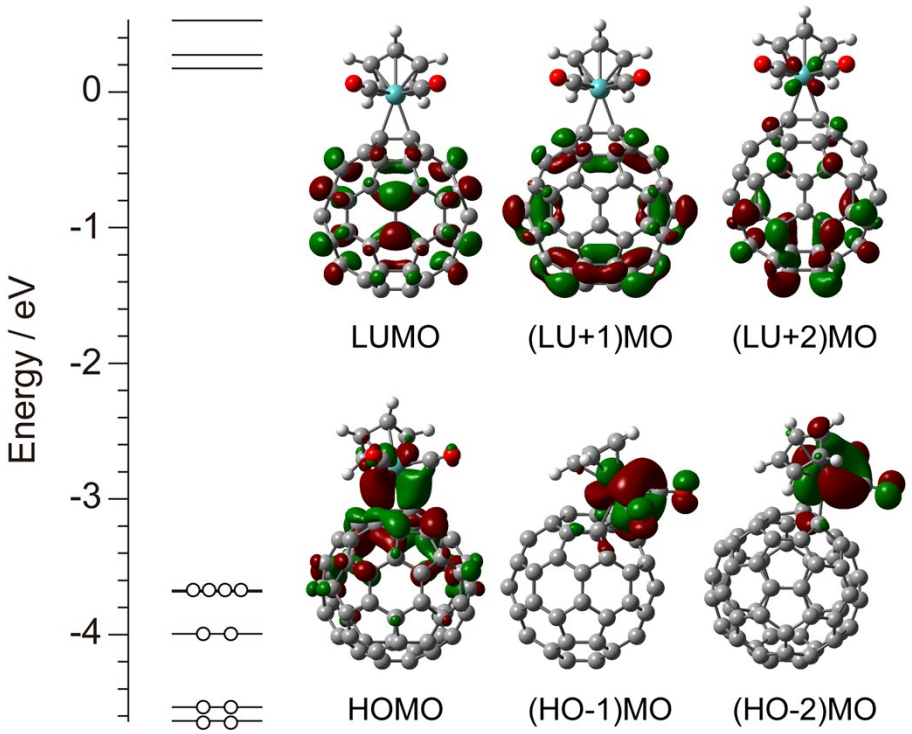

Fig. S9 Energy diagrams for the frontier Kohn-Sham orbitals of the ^1A state in $\{CpMo(CO)_2(\eta^2\text{-}C_{60})\}^-$ calculated at the RCAM-B3LYP-D3 levels of theory.

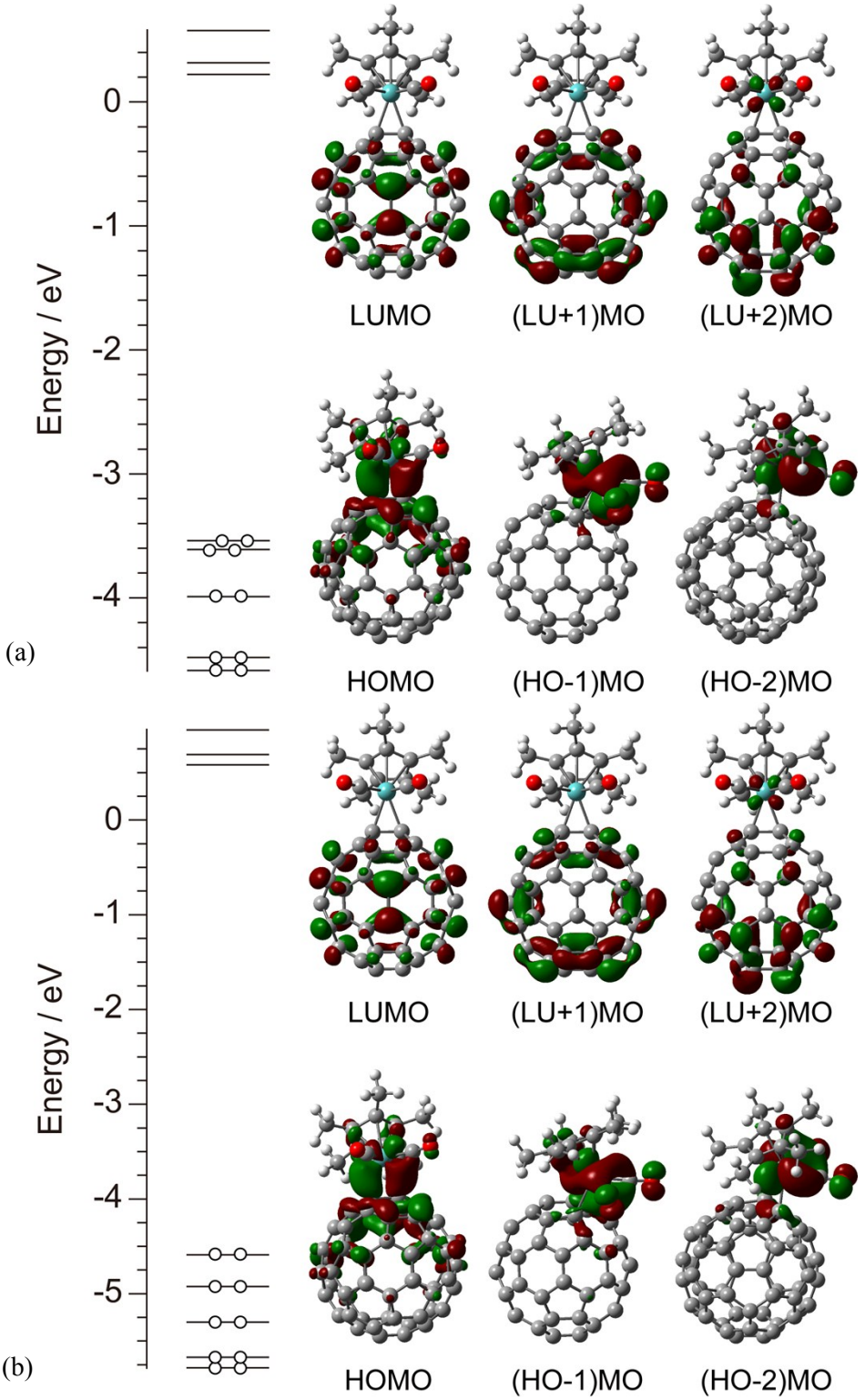

Fig. S10 Energy diagrams for the frontier Kohn-Sham orbitals of the ^1A state in $\{Cp^*Mo(CO)_2(\eta^2\text{-}C_{60})\}^-$ calculated at the (a) RCAM-B3LYP-D3 and (b) RM11/cc-pVTZ-PP/cc-pVDZ levels of theory.

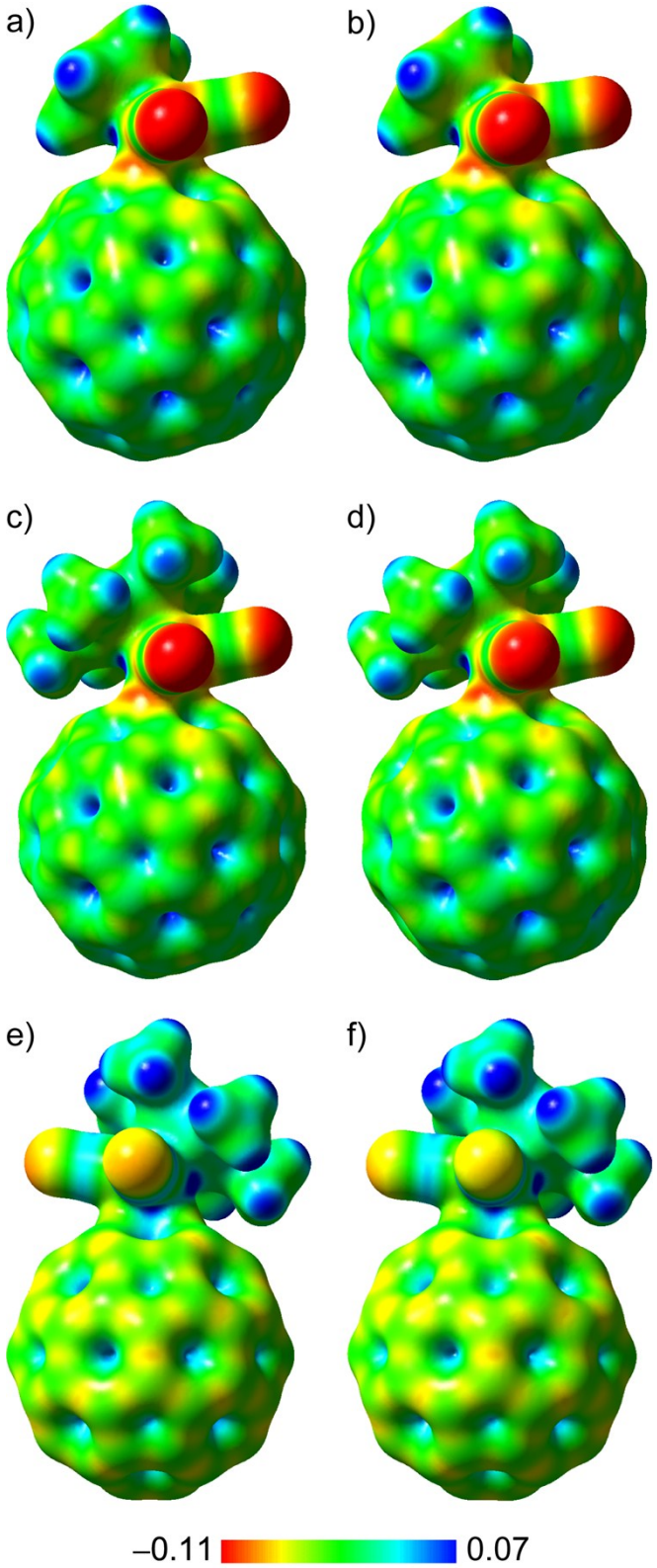

Fig. S11 Electrostatic potential maps on the 0.02 electron/au^3 of electron density surface in $\{CpMo(CO)_2(\eta^2\text{-}C_{60})\}^-$ for the ^1A states at the (a) RCAM-B3LYP-D3 and (b) RM11, and $\{Cp^*Mo(CO)_2(\eta^2\text{-}C_{60})\}^-$ for the ^1A states at the (c) RCAM-B3LYP-D3 and (d) RM11 and the ^3A states at the (e) UCAM-B3LYP-D3 and (f) UM11/cc-pVTZ-PP/cc- pVDZ levels of theory.

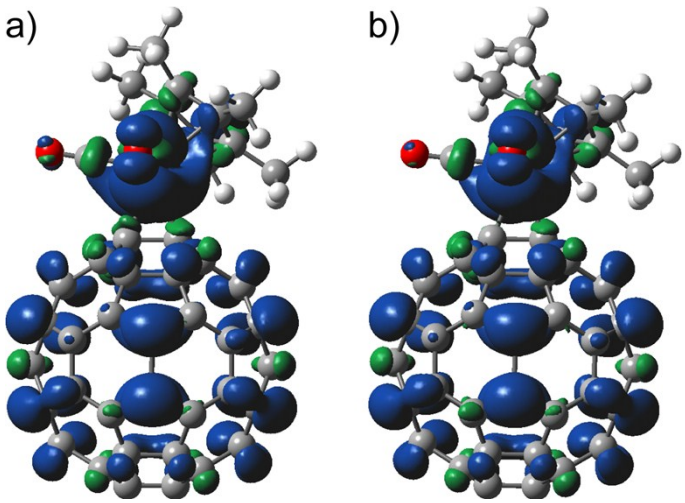

Fig. S12 The isosurface plots on spin density distribution of the ^3A state in $\{Cp^*Mo(CO)_2(\eta^2\text{-}C_{60})\}^-$ calculated at the (a) UCAM-B3LYP-D3 and (b) UM11/cc-pVTZ-PP/cc-pVDZ levels of theory. The isosurface value is 0.0009 electron/au^3. The isosurfaces in blue and green denote the positive and negative spin density, respectively.